Lithuanian Journal of Physics
Vol. **64**, No. 2, pp. 122–138 (2024)
ISSN 1648-8504 eISSN 2424-3647
DOI: https://doi.org/10.3952/physics.2024.64.2.5

RECENT EVOLUTION OF THE STAR CLUSTER POPULATION IN THE ANDROMEDA'S DISK

M. Čeponis [a], R. Stonkutė [a, b], and V. Vansevičius [a]

[a] *Center for Physical Sciences and Technology, Saulėtekio 3, 10257 Vilnius, Lithuania*
[b] *Astronomical Observatory of Vilnius University, Saulėtekio 3, 10257 Vilnius, Lithuania*
Email: vladas.vansevicius@ftmc.lt

Received 8 March 2024; revised 25 April 2024; accepted 26 April 2024

The most accurate parameters of star clusters are determined by analyzing colour-magnitude diagrams (CMDs) constructed from their member stars. The recent study applying this method to the analysis of the Panchromatic Hubble Andromeda Treasury (PHAT) survey star clusters includes objects up to ages of 300 Myr. In this study, we aim to extend a sample of star clusters with parameters determined based on CMDs of individual stars to older ages, up to ~700 Myr. We have developed an isochrone fitting procedure for CMDs of resolved and semi-resolved clusters to determine their parameters. The Bayesian approach is employed in determining star cluster ages and interstellar extinctions. We determined ages and extinctions for a sample of 854 star clusters from the M31 PHAT survey. We found that the star formation rate in the M31 galaxy was rather constant during the last ~130 Myr; however, a strong cluster formation episode occurred ~220 Myr ago, and can be attributed to the predicted passage of the M32 galaxy through the Andromeda's disk.

Keywords: galaxies, Andromeda, M31, star clusters

1. Introduction

Star clusters are one of the key elements in understanding star formation processes and, consequently, the formation and evolution of their host galaxies. Most stars form in embedded star clusters [1] and, although most of these stellar structures dissociate over the first few Myrs, the remaining population of gravitationally bound clusters give a direct insight into the inner workings of star formation. Studies of nearby galaxies have shown that there is a correlation between the star formation rate surface density and the star cluster formation efficiency – the fraction of stellar mass formed in long-lived star clusters [2, 3]. These findings reveal that star clusters are tightly connected with their formation environment and trace back the characteristics of past star formation episodes in galaxies. Therefore, an accurate cluster parameter determination is crucial in understanding the processes governing star formation.

One of the best research sites for unravelling the inner workings of star formation processes within galaxy disks is the Andromeda (M31) galaxy. It is the largest spiral galaxy in the Local Group with a complex star formation history and multiple stellar structures [4, 5]. An extensive Panchromatic Hubble Andromeda Treasury (PHAT) survey [6] had covered a significant portion of the galaxy disk and enabled the production of the largest star cluster catalogue of M31 [7] with 2753 confirmed objects. Using photometric data of resolved stars, Ref. [2] derived parameters for clusters younger than 300 Myr. However, knowing parameters of older clusters would allow the study of longer galaxy evolution processes and also of the dissipation of stellar clusters themselves. In a wider age range, the PHAT clusters were studied based on

integrated photometry [8, 9]; however, the accuracy of clusters parameters was not satisfactory. Reference [10] discussed the limitations of the accuracy of star cluster parameters derived from integrated broad-band photometry.

A new version of the PHAT survey stellar photometry catalogue has been recently published [11]. The higher accuracy of stellar photometry and the increased number of resolved sources in the new catalogue edition has enabled us to derive parameters for star clusters of ages up to 700 Myr.

In this paper, we present a colour-magnitude diagram (CMD) fitting method for resolved and semi-resolved cluster analysis and derive parameters for a sample of 854 clusters in the M31 galaxy. We employ the Bayesian approach to decontaminate cluster star samples and to determine age and extinction parameters from multi-colour photometry data of individual cluster stars. Our work complements previous studies of M31 clusters [2] by providing parameters for older objects.

The paper is organized as follows. We begin with a brief description of observational data and the cluster sample used in Section 2. The method applied for determining cluster parameters is presented in Section 3. Tests with artificial star clusters to assess the reliability of the cluster analysis method are described in Section 4. In Section 5, we present and discuss the results of cluster analysis. Finally, the conclusions are given in Section 6.

2. Observation data and the cluster sample

In this study, we employed data from the PHAT survey [6], which covers a significant portion of the M31 disk – from the very centre to the outermost north-eastern regions. We used the final legacy version of the PHAT survey's stellar photometry of 138 million sources [11]. The catalogue provides measurements in six passbands, covering a spectral region from near-ultraviolet to near-infrared: the *F*275*W* and *F*336*W* passbands from the Wide Field Camera 3 UVIS channel (WFC3/UVIS), the *F*475*W* and *F*814*W* passbands from the Advanced Camera for Surveys (ACS/WFC), and the *F*110*W* and *F*160*W* passbands from the Wide Field Camera 3 IR channel (WFC3/IR).

We selected stars with measured magnitudes above the 30% completeness limit in the *F*475*W* passband and at least in one other passband (*F*336*W* or *F*814*W*). We used the *F*110*W* and *F*160*W* passbands solely for field decontamination, excluding them from cluster parameter determination due to their lower photometric quality and reduced sensitivity to variations in star cluster parameters. The remaining four passbands cover a sufficiently wide range of the spectrum to accurately determine star cluster ages and extinction values.

We began with a sample of 1181 clusters, sourced from the Andromeda Project cluster catalogue [7], that were analyzed in Ref. [12]. We discarded clusters older than 1 Gyr for which we cannot determine reliable parameters due to photometry completeness limits. This left us with a sample of 854 clusters. For full details on cluster selection criteria see Refs. [9, 12, 13]. We used cluster centre coordinates and photometric aperture radii R_{ap} reported in Ref. [12]. In general, the sample should contain only star clusters with high-quality photometric measurements. Therefore, clusters in the very centre of the galaxy are omitted from analysis, as can be seen in the map of our cluster sample distribution (Fig. 1). Nonetheless, they cover a wide range of different environments, from dense star-forming regions to relatively uncrowded outer disk areas.

3. Derivation of cluster parameters

3.1. Overview of existing methods

The main problems in deriving star cluster parameters using photometric measurements of individual stars arise due to the contamination of cluster stars by the foreground and (or) background field stars (hereinafter field stars), as well as age–extinction and age–metallicity degeneracies of cluster parameters. The simplest and most common method to bypass these problems is matching isochrones by eye on a CMD [14–16]. Even though this method gives reliable results if done by experts, there is still a problem of repeatability because of the subjective matching process, and it is very inefficient, especially when applied to large samples of star clusters.

Another widely used method to determine cluster parameters from stellar photometry data is a comparison of artificially generated CMDs of

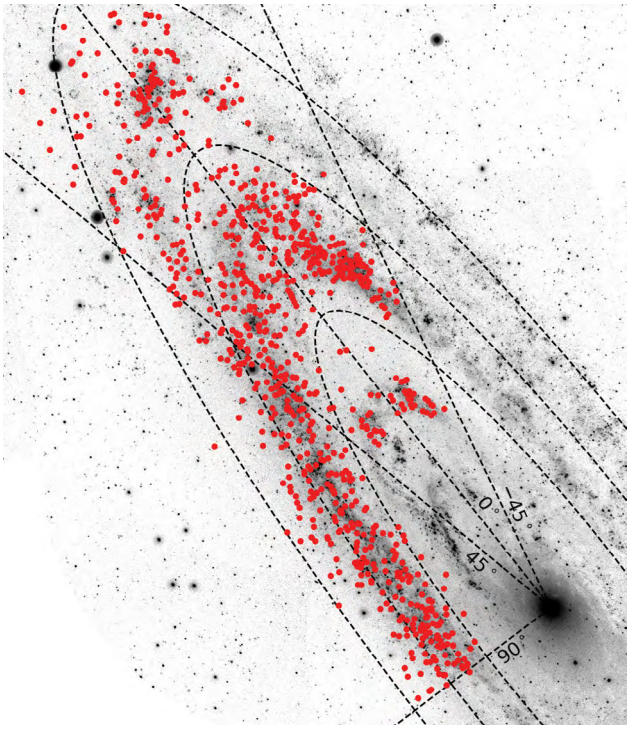

Fig. 1. Spatial distribution of the 854 clusters analyzed in this paper overlaid on a GALEX NUV image of M31. Dashed ellipses mark circles of 9, 14 and 19 kpc radii on the deprojected galaxy disk. Dashed straight lines mark angles corresponding to the indicated values in degrees on the deprojected galaxy disk. The zero angle corresponds to the direction of the major axis. North is up and east is left.

synthetic simple stellar populations to the observed data [17–19]. By employing this method, field contamination can be easily taken into account through the inclusion of a model representing the field star population in the artificially generated CMD. Nonetheless, this method is still sensitive to the level of contamination by field stars. Also, the results heavily depend on knowing the actual distributions of photometric errors and completeness, which is not always the case for observations of extragalactic clusters. In such systems, the density of stars increases rapidly from the outskirts of the cluster to the centre and, accordingly, the quality of photometric measurements deteriorates. This makes it hard to determine the real distributions of photometric errors and completeness.

There are also many methods for distinguishing cluster stars from field stars. The most accurate ones incorporate not only the photometric measurements but also the proper motions of stars in cluster areas [20, 21]. However, such measurements are usually not available for extragalactic clusters. When only the photometric measurements are available and the cluster is not heavily contaminated by the field star population, one simple solution is to discard stars that deviate from the main sequence (MS) by a certain distance in CMDs [22, 23]. However, most star clusters are too contaminated to use this method. For such cases, more sophisticated algorithms can be employed. Most of them rely on comparing the cluster stellar density and CMD distributions to those of field stars in various ways [24–26]. Nevertheless, it is also possible to decontaminate a cluster population without solely relying on the comparison of stellar distributions to neighbouring field regions. This can be achieved by analyzing the clustering of stars in various measured parameter spaces, as demonstrated in Refs. [27] and [28].

However, the decontamination of the cluster star sample from field stars alone is insufficient to determine cluster parameters. Cluster decontamination algorithms are often used in combination with isochrone fitting [29–31] or synthetic cluster fitting [32, 33] to determine cluster parameters.

We developed our own method for decontaminating star clusters and determining parameters, tailored for resolved or semi-resolved extragalactic objects. It consists of two parts: a) the recognition of field stars; b) the fitting of theoretical isochrones to a clean cluster star sample to determine the most probable cluster parameters. Although both parts of the method can be used separately for their corresponding purposes, they are specifically designed to be used in conjunction to ensure the robustness of the final results. However, it has been shown that in principle, clusters' parameters can also be determined with convolutional neural network methods [34]. Considering the rapid advancements in this field, better accuracy might be achieved in the near future.

3.2. Field star decontamination

We developed a two-step method to remove field stars from the clusters' aperture. Firstly, we assign a likelihood score of cluster membership to each star within a cluster-centred aperture (R_{ap}) using a modified version of the method described in Ref. [33]. Secondly, we use these scores to calculate

probabilities of being cluster members by comparing star density distributions in selected CMDs to those of field stars using sliding windows of various sizes. Finally, we discard any star with a cluster membership probability below a cut-off value.

Let us assume that the sample of stars located within the cluster's aperture, R_{ap} (sample A), consists of cluster members (subsample C) and field stars (subsample F). Then the problem of separating these two sets of stars can be reduced to this: what is the probability of any star in the sample A to be a cluster member ($\in C$) or a field star ($\in F$)? This can be separated into two hypotheses: H_1 – the star is a cluster member ($\in C$); H_2 – the star is a field star ($\in F$). Because these hypotheses are exclusive and exhaustive, at least one of them must be true; therefore, we need to find only the probability of H_1 to separate the two sets of stars.

By employing Bayes' theorem, we can calculate $P(H_1|D)_i$ – the probability, given the data D (i.e. the photometry for all stars), that H_1 is true for a randomly selected star i from the sample A; this probability signifies the likelihood of the star being a cluster member. For H_1 prior, we compare the star density parameter in the vicinity of the selected star, ρ_i, and the average density parameter of field stars, $\langle\rho\rangle_B$, determined from the field star region outside of the cluster's aperture (sample B): $P(H_1) = \rho_i/(\rho_i + \langle\rho\rangle_B)$. In this study, we selected an annulus between 2.0 and 3.5 $\cdot$ R_{ap} to represent the field star population (sample B) for each corresponding cluster.

Such a range of radii was chosen because the field region must be sufficiently distant from the cluster's centre to ensure that there is no significant number of actual cluster's stars in the field star sample. Additionally, it must not be too far from the cluster to ensure that the sample is still representative of the field star population inside the cluster's aperture.

For H_2, we simply use the inverse of H_1 prior: $P(H_2) = 1 - \rho_i/(\rho_i + \langle\rho\rangle_B)$. We calculate the star density in the vicinity of a given star i as follows:

$$\rho_i = \frac{1}{N_X}\sum_{j=1}^{N_X}\exp\left[\frac{-4((\alpha_i-\alpha_j)^2+(\delta_i-\delta_j)^2)}{R_{\rm ap}}\right]. \quad (1)$$

Here X is a sample of stars separated from the star i by less than 0.5 $\cdot$ R_{ap}. The parameters (α, δ) represent right ascension and declination, measured in arcseconds, respectively.

Combining everything mentioned above with the likelihoods $L_{C,i} = P(D|H_1)_i$ and $L_{F,i} = P(D|H_2)_i$ for star i, we get the final form of the cluster membership probability,

$$P(H_1 \mid D)_i = \frac{L_{C,i}}{L_{C,i} + (\langle\rho\rangle_B/\rho_i)L_{F,i}}, \quad (2)$$

where the likelihood of star i is calculated as

$$L_{Y,i} = \frac{1}{N_X}\sum_{j=1}^{N_X}\frac{1}{\sigma_m(i,j)\sigma_c(i,j)} \exp\left[\frac{-(m_i-m_j)^2}{2\sigma_m^2(i,j)}\right]\exp\left[\frac{-(c_i-c_j)^2}{2\sigma_c^2(i,j)}\right]. \quad (3)$$

Here $Y \in \{C, F\}$ and $X \in \{A, B\}$, the parameters (m, c) represent magnitude and colour, and (σ_m, σ_c) denote their respective photometric uncertainties of the form

$$\sigma_m^2(i,j) = \sigma_m^2(i) + \sigma_m^2(j),\ \sigma_c^2(i,j) = \sigma_c^2(i) + \sigma_c^2(j). \quad (4)$$

However, if photometric uncertainties are not very well known, as it is usually the case in dense extragalactic clusters, it is better to not use them at all (set $\sigma_m = 1$ and $\sigma_c = 1$), as we did in this work. This method is sensitive to the ratio of uncertainty values, and any inaccuracy in determining photometric uncertainty can skew the results.

One can try to use Eq. (2) to separate cluster members from non-members, but this probability works poorly in the cases of clusters that are highly contaminated by field stars (i.e. the number of cluster members is equal to or less than the number of field stars inside the cluster's aperture). To circumvent this problem and make the method more robust, we use an approach of sliding windows of various sizes in conjunction with the probabilities that we got from Eq. (2).

We start by setting a square window sized 0.5 × 0.5 mag^2 in the $F475W$ vs ($F475W$–$F814W$) CMD and then identify stars in both sample A and sample B that fall within this window. From the number of field stars inside this window and the ratio of cluster and field star region areas, we determine the number of field stars in the sample A located inside this window. We omit the estimated number of field star candidates by selecting

the ones with the lowest probability values (Eq. 2) from the star sample of the window under consideration, and mark the remaining stars as probable cluster members. Then, we slide the window by a quarter of its size and repeat the procedure until we check all stars in the sample *A*. The same procedure is then repeated with an increased window size. We use square windows of sizes from 0.5×0.5 to 5.0×5.0 mag^2 by increasing the side of the window by 0.5 mag in each iteration. This procedure is also performed in the $F336W$ vs ($F336W$ $F475W$) and $F110W$ vs ($F110W$ $F160W$) CMDs. Finally, we count how many times each star in the sample *A* was marked as a probable cluster member and how many times in total it was checked. We assign the ratio of these two values as the probability for a star to be a cluster member. An example of the APID 0031 cluster decontamination from field stars is shown in Fig. 2.

In this study, we use a probability cut-off value of 0.9 to select only the most likely cluster members because the method that we use for cluster parameter determination (see Subsection 3.3) gives the best results in the cases of the least contaminated samples and is rather insensitive to the total number of stars used. However, when using this decontamination method in conjunction with other methods, one should exercise caution and optimize the probability cut-off value for the problem at hand.

To ensure the quality of field decontamination, we visually inspected each cluster's CMDs for bright stars strongly deviating from the isochrones (suspected of being not cluster members), that did not get discarded by the method, and removed them interactively. Such bright stars are rare, and the corresponding part in the CMD of the field star sample is usually too sparse to enable the algorithm to distinguish statistically between field stars and cluster stars.

3.3. Cluster parameter determination

A probabilistic approach was used to determine clusters' parameters. The photometric data of each star located within the cluster's aperture R_{ap} are compared to the corresponding data in a database of stellar models. This way, the probability distribution function (PDF) is calculated over a range of extinction and age values, which is then used to determine the best fit parameter set for the cluster.

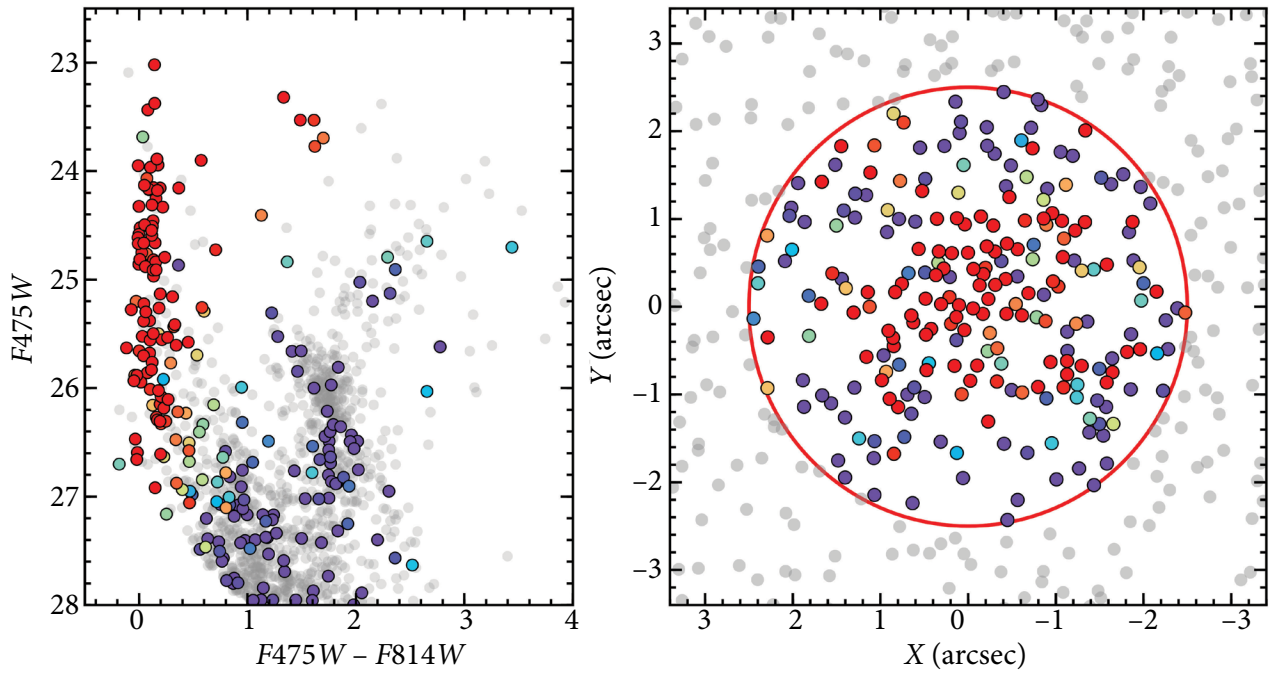

Fig. 2. The CMD and the coordinate map show the results of the APID 0031 cluster decontamination from field stars. Stars in sample *A* (located within the cluster centred aperture) are marked by colour-coded dots according to their cluster membership probabilities (colours from red to blue represent probabilities from the highest to the lowest ones). Field stars located outside of the cluster's aperture are marked by grey dots.

In this study, we adopted a distance modulus of the M31 galaxy of $m - M = 24.47$ [35], an initial mass function *IMF* from Ref. [36] for masses from 0.1 to 120 $M_\odot$, a Milky Way interstellar extinction curve ($R_V = 3.1$), and stellar models from the PAdova and tRieste Stellar Evolutionary Code (PARSEC)-COLIBRI release v1.2S [37, 38]. Throughout this paper, we use a fixed metallicity value of $[M/H] = 0$ in accordance to present day gas metallicity observations within M31 [39, 40]. Also, during cluster parameter fitting, we do not take into account binary stars since our tests with artificial star clusters showed that their effect is negligible compared to that of other error sources. We used photometric error dependences and completeness functions derived from the artificial star tests (AST) for the final legacy version PHAT survey stellar photometry provided in Ref. [11].

In our analysis, we use individual star photometry data in four passbands – *F*275*W*, *F*336*W*, *F*475*W* and *F*814*W* – available from the PHAT survey (see Section 2). We exclude stars with *F*475*W* magnitudes below the 30% completeness limit from cluster parameter fitting. We also exclude stars with magnitudes in both *F*336*W* and *F*814*W* passbands below this completeness limit. For 74 overly dense clusters (9% of the sample), we excluded central parts where the majority of stars are poorly measured due to unresolved optical blends.

For each selected star in a cluster, we calculate an individual PDF $P_i(A_V, t)$ over wide ranges of extinction A_V and age t values. For extinction, we use the range of $A_V = 0.0$–2.5 mag with a step of 0.05 mag, and for age we use the range of $\log(t/\mathrm{yr}) = 6.6$–$10.1$ dex with a step of 0.05 dex to cover all possible cluster values with a sufficient parameter resolution.

The PDF $P_i(A_V, t)$ of a star is calculated by comparing its position in a CMD, $\boldsymbol{F}_i = (m_i, c_i)$, to the individual points $\boldsymbol{L}_j(M_j, A_V, t) = (m_j, c_j)$ of a theoretical isochrone of the age t reddened by the extinction of A_V. This is done by assuming Gaussian photometric errors and an *IMF* that is integrated over a small interval of initial stellar masses M_j, corresponding to an individual point of an isochrone. Calculations are done over all isochrone points and summed up to arrive at the final PDF of an individual star *i*:

$$P_i(A_{V,t}) = N_i^{-1} \sum_j G(\boldsymbol{F}_i, \boldsymbol{L}_j) \int_{M_j} IMF(M)\mathrm{d}M, \quad (5)$$

$$G(\boldsymbol{F}_i, \boldsymbol{L}_j) = \frac{\exp[-\frac{1}{2}(\boldsymbol{F}_i - \boldsymbol{L}_j)^{\mathrm{T}} \Sigma_i^{-1} (\boldsymbol{F}_i - \boldsymbol{L}_j)]}{2\pi\sqrt{\det \Sigma_i}}, \quad (6)$$

$$N_i = \sum_{A_V} \sum_t P_i(A_V, t). \quad (7)$$

Here $G(\boldsymbol{F}_i, \boldsymbol{L}_j)$ is the multivariate Gaussian distribution function; Σ_i is the error covariance matrix for the photometric measurements $\boldsymbol{F}_i$, and N_i is the normalization constant over all allowed A_V and t parameter values.

To circumvent the effects of differential extinction, binary stars, and optical blends, we double the difference $\boldsymbol{F}_i$–$\boldsymbol{L}_j$ in Eq. (6) for the main-sequence (MS) stars that are bluer than the MS of the isochrone. This forces the method to be less sensitive to red stars, essentially fitting isochrones as envelope lines for MS stars.

We multiply and renormalize all PDFs, $P_i(A_V, t)$, of the cluster stars to arrive at a PDF for the whole cluster:

$$P_{\mathrm{C}}(A_V, t) = N_{\mathrm{C}}^{-1} \prod_i P_i(A_V, t), \quad (8)$$

$$N_{\mathrm{C}} = \sum_{A_V} \sum_t P_{\mathrm{C}}(A_V, t). \quad (9)$$

For each cluster, we calculate two PDFs from *F*475*W* vs (*F*475*W*–*F*814*W*) and *F*814*W* vs (*F*475*W*–*F*814*W*) CMDs and multiply them with each other. The maximum of this PDF is used to get the best fit extinction value. Then we calculate another PDF from *F*336*W* vs (*F*275*W*–*F*336*W*) CMD but with an already fixed determined extinction value. This is due to the less precise measurements in UV, which make accurate extinction derivation challenging. Nonetheless, UV passbands help us to constrain cluster ages when the main-sequence-turn-off (MSTO) position is not clear in cases of young clusters. We multiply this UV PDF with the previous one to get the final PDF, the maximum of which is set as the best estimate of the cluster's age.

We assign uncertainties based on the 16th and 84th percentiles derived from the marginalized 1D PDFs of age and extinction. To ensure the reliability of derived cluster parameters, we plotted CMDs of each cluster to visually check how well isochrones fit the data (Fig. 3), and for ~15% of the clusters, we adjusted automatically derived

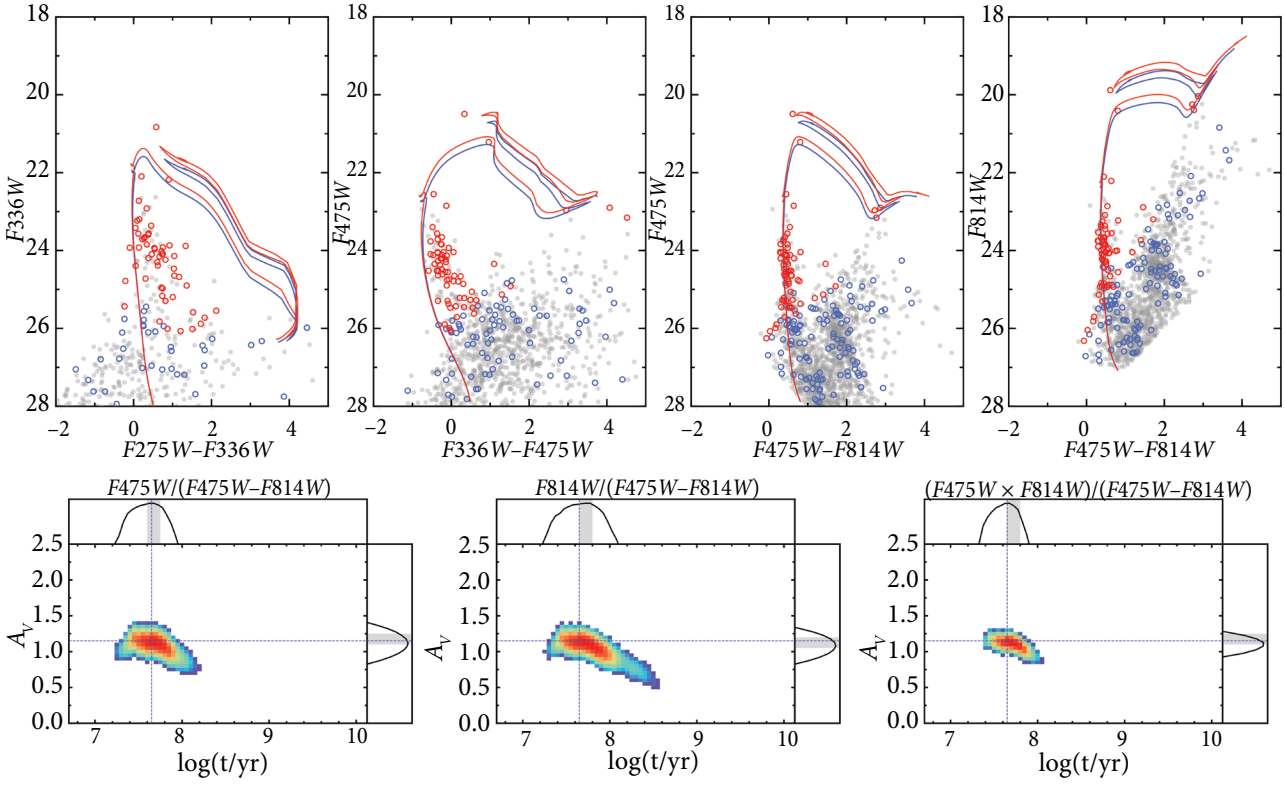

Fig. 3. CMDs and PDF distributions of the cluster APID0093. CMDs include all stars that lie within the aperture of R_{ap}. Red circles show the cluster stars selected for the analysis as true cluster members. Blue circles show the stars with magnitudes below 30% completeness limits or rejected as contaminants belonging to the field star population. The field stars lying in a ring of (2.0–3.5) R_{ap} are marked as grey dots. The cluster parameters, derived taking into account all CMDs, are $\log(t/\mathrm{yr}) = 7.65$ and $A_V = 1.15$ (the red isochrone); the blue isochrone is based on the parameters determined from a single CMD, *F*475*W* vs (*F*475*W*–*F*814*W*). For a visual clarity PDF distributions are shown in a logarithmic scale. Grey areas in the marginalized 1D PDF distributions show uncertainties of the fitting results, corresponding to the 16th and 84th percentiles.

parameters. In most of these cases, either the field stellar population is younger than the cluster and the algorithm has problems in determining which MSTO belongs to the cluster, or the cluster is projecting on a dense field of old stars and the tip of red-giant branch stars contaminate the sample of cluster members.

4. Tests based on artificial star clusters

To assess the reliability of the developed method for determining cluster parameters, we carried out extensive tests with artificially generated star clusters. To generate artificial star clusters, we used the same isochrones, *IMF*, and other parameters as the ones used to derive parameters of real clusters described in Subsection 3.3. Initial masses of cluster members are randomly drawn from the *IMF* [36] until the required cluster mass is reached. The stellar masses are then used to interpolate absolute magnitudes from the isochrones in all six passbands used in the PHAT survey.

All generated cluster stars were reddened by the assumed extinction values, and their absolute magnitudes were corrected for the distance modulus of M31. Then, for all stars (in each passband), depending on their magnitudes, we assigned probabilities not to be measured, which are calculated based on the known completeness function [11]. Using these probabilities, we discarded a corresponding part of magnitudes to imitate measurement completeness effects. Random Gaussian errors were then applied to the magnitudes in order to imitate real photometric measurements. These errors were generated based on the artificial star test results provided for the legacy version of PHAT stellar photometry [11].

To simulate realistic star clusters, we added real field star populations to the artificial cluster stars. For each artificial cluster, we randomly selected

one out of 50 different field star populations surrounding real clusters analyzed in this study (stars in a ring of 2.0–3.5 · R_{ap} centred on clusters). Then, we randomly selected a 4/33rd part (it is equal to the ratio of the clusters' aperture areas to the areas of field star regions) of stars to represent the population of field stars residing within the cluster's aperture of an R_{ap} radius so that the realistic contamination by field stars is mimicked. Also, we generated artificial stars' sky coordinates using a simple Gaussian distribution with a standard deviation equal to half the cluster's aperture radius R_{ap}. This was done to fully simulate the characteristics of real star clusters.

We generated a grid of artificial star clusters with eight age values log(t/yr) = 7.0, 7.5, 8.0, 8.3, 8.5, 8.7, 8.85, 9.0, three mass values log(M/M$_\odot$) = 2.5, 3.0, 3.5, and three extinction values A_V = 0.0, 0.5, 1.0. For each parameter combination, 50 clusters were generated using different random seeds for *IMF* sampling as well as for completeness and errors imitations. Then, in the same way as described in Section 3, we applied our method to determine ages and extinctions of these clusters.

The results of artificial cluster tests for the data of PHAT survey quality are shown in Fig. 4. The effects of age–extinction degeneracy in cluster parameter determination are visible (panels (s), (t), (u)). They are stronger in the cases of low-mass clusters ($\lesssim$300 M$_\odot$) when post-main-sequence stars are absent due to *IMF* stochasticity. However, we can conclude that our method reliably determines ages and extinctions for clusters with masses of $\gtrsim$1000 M$_\odot$ and for ages up to almost 1 Gyr. The scatter of results, defined as the 16 and 84th percentiles (shown with error bars), increases moderately with age and more substantially with higher extinction values and lower cluster masses. These uncertainties could be considered as realistic expectations of parameter accuracy in the case of real clusters.

5. Results and discussion

We have determined ages and interstellar extinctions for a sample of 854 star clusters in the M31 galaxy. An example of templates used for the visual quality control of the determined cluster parameters is shown in Fig. 3. Additionally, we estimated rough cluster masses based on a single stellar population (SSP) approximation.

The distribution of derived extinction values versus ages is shown in Fig. 5. In total, 155 clusters are older than 300 Myr, i.e. ~18% of the entire sample. The derived extinctions correlate with ages – younger clusters tend to have higher extinctions than older ones. This is most likely due to younger clusters' tendency to reside closer to star-forming regions in denser interstellar environments. Consequently, they are more likely to be located inside or behind dusty gas clouds. Nonetheless, some older ($\gtrsim$500 Myr) clusters also have elevated extinction (up to $A_V \sim 1.0$), which can be explained by them being on the other side of the galaxy disk, behind a layer of diffuse interstellar matter.

To verify the reliability of our results, we compare derived ages and extinction values with the star cluster data published in Ref. [2] and further supplemented in Ref. [43]. In total, 682 clusters are present for comparison with our data (Fig. 6). Most derived values are in agreement with each other with a small mean difference between ages, $\langle\Delta\log(t/yr)\rangle \sim 0.09$ dex, and extinction values, $\langle\Delta A_V\rangle \sim 0.10$ mag. Our method favours slightly older cluster ages and lower extinctions. The degeneracy of these cluster parameters is well known employing integrated photometry [45, 46]; however, the same degeneracy seems to apply even in the analysis of colour–magnitude diagrams (Fig. 4). However, there are some outliers with large age differences most likely caused by low numbers of cluster stars and (or) high background field densities. Also, unlike Ref. [2], in our analysis, we incorporated not only measurements in the *F*475*W* and *F*814*W* passbands, but also data obtained in the UV passbands which are least affected by field star contamination. This might have led to a better distinction between field stars and cluster members in our analysis.

The mass of clusters in the solar-mass units M/M$_\odot$ was calculated based on the absolute magnitudes *F*475*W* of the solar metallicity SSP models [37, 38] dereddened by applying determined extinction values, as well as determined cluster ages and integrated aperture magnitudes [12]. The comparison of the determined masses of clusters from our sample with the published data based on the same HST observations [2, 43] shows a good agreement without systematic biases. The differential cluster age distribution

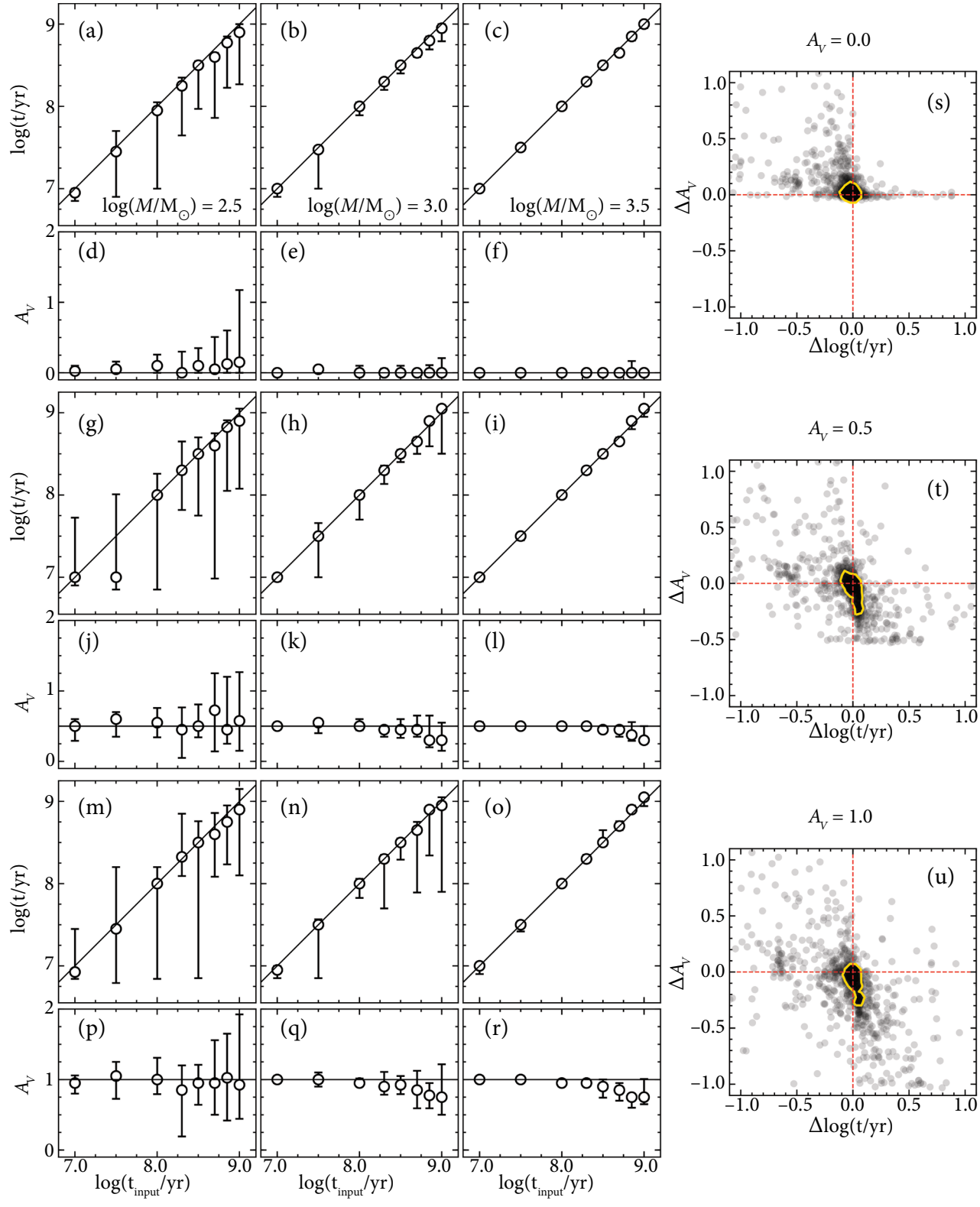

Fig. 4. The results of artificial star cluster tests: distributions of recovered parameters – ages and extinctions vs input ages of artificial clusters. Top two rows for clusters with extinction $A_V = 0$; middle two rows for $A_V = 0.5$; bottom two rows for $A_V = 1.0$. Clusters were generated with three different mass values: 300 $M_\odot$ in the left column; 1000 $M_\odot$ in the middle column; 3000 $M_\odot$ in the right column. Open circles mark median values and whiskers indicate the 16th and 84th percentiles. For each combination of age, extinction and mass, sets of 50 artificial clusters were generated. Panels (s), (t) and (u) show the differences of derived and input extinction values vs the differences of ages in the cases of three input extinction values for models of all ages and masses merged. The yellow contour includes 68% of data.

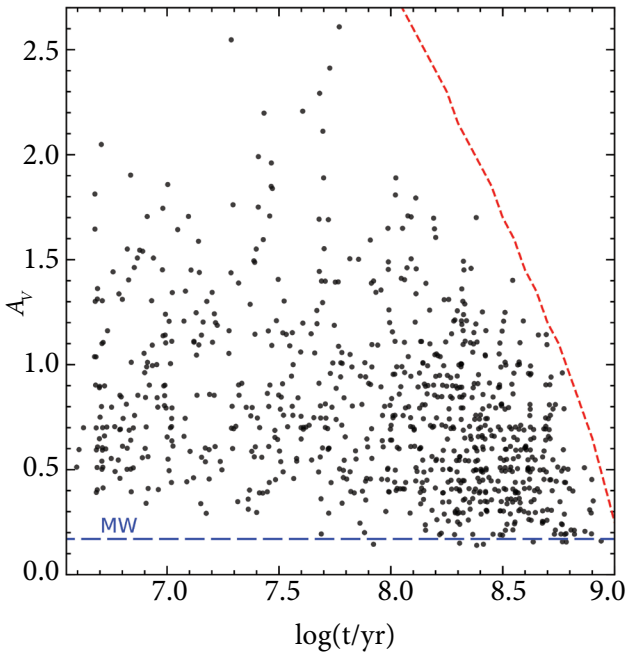

Fig. 5. Derived cluster ages versus extinction values. The blue dashed line indicates the Milky Way dust attenuation value of A_V = 0.17 in the direction of the M31 galaxy [41, 42]. The red short dashed line shows the cluster selection limit assuming the MSTO tip of $F475W \lesssim 25$ mag. The correlation of extinctions with cluster ages is noticeable – the extinction of older clusters is lower on average. Note the numerous population of yet undispersed star clusters (or stellar associations) at the youngest ages log(t/yr) ≲7.

shown in Fig. 7 is drawn for clusters more massive than 800 $M_\odot$ to avoid uneven selection effects over a wide range of considered ages, ≲700 Myr. The massive clusters (>800 $M_\odot$) were selected for further analysis because their detection completeness level is approximately the same regardless of the clusters' ages up to ~700 Myr.

The distribution is primarily characterized by an exponential decline due to the cluster evolutionary fading. Subsequently, around ages of 300 Myr, the effects of cluster disruption become dominant [47, 48]. However, due to the completeness effects taking over for older clusters, we cannot accurately determine the cluster disruption rate; therefore, we plotted the estimate derived for the south-western part of the M31 disk [44, 49, 50]. Their derived cluster evolutionary fading rate fits our results very well indicating that the cluster formation rate during the last ≲130 Myr was rather constant. The noticeable feature in the cluster age distribution is at (220 ± 40) Myr age, indicating an enhanced episode of cluster formation. It might have been induced by an interaction with the M32 galaxy [51–53]. In Ref. [51] it was suggested that M32 collided with M31 almost head-on about 210 Myr ago, and then passed through the M31 disk again about 110 Myr ago. However, we do not see enhanced star formation around 110 Myr,

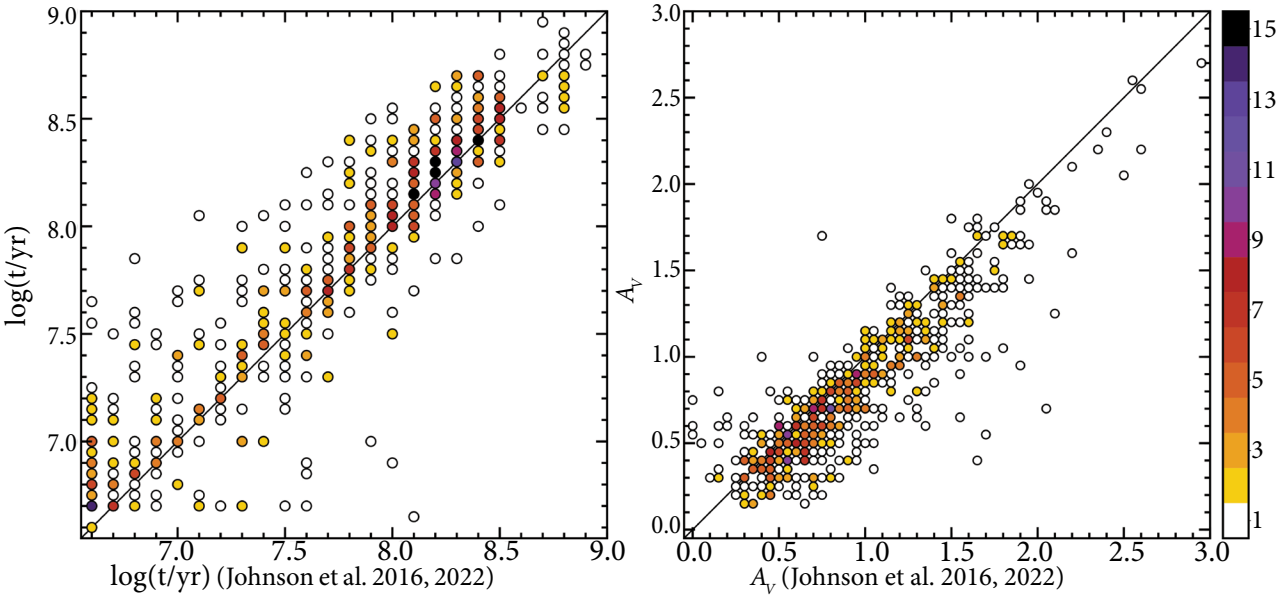

Fig. 6. Derived cluster ages (left) and extinctions (right) versus published values [2, 43]. A bias of ages and extinctions is visible: our method favours slightly lower extinction values and older cluster ages in accordance with the parameter degeneracy shown in Fig. 4. The colours of dots correspond to the colour-bar indicating the number of clusters overlapped at the same position.

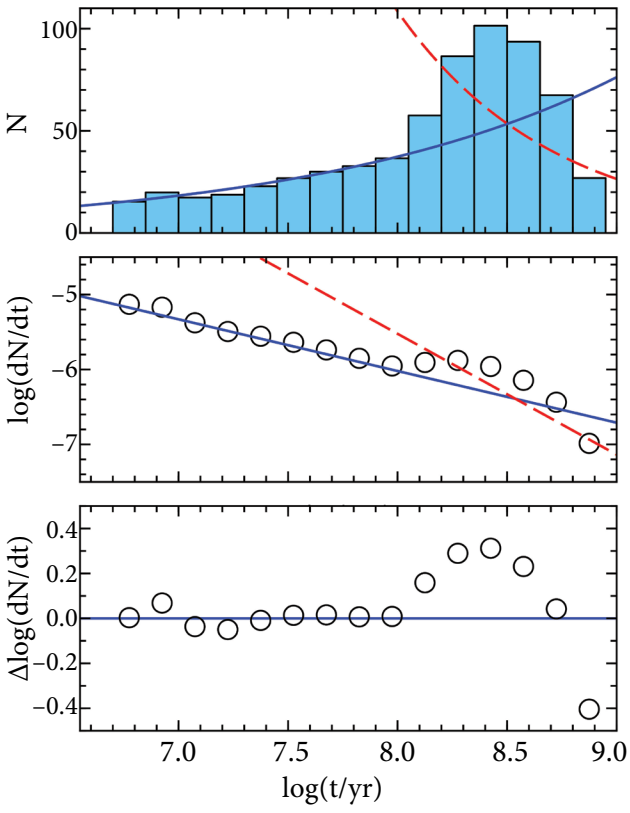

Fig. 7. Top: the distribution of the derived ages of clusters more massive than 800 $M_{\odot}$. Middle: the differential distribution of cluster ages (the same sample as above) shown by open circles (the size indicates the uncertainty of data binning). The solid and the dashed lines show the cluster evolutionary fading rate and the cluster disruption rate, respectively. Slope values for these lines are taken from Ref. [44]. Bottom: the differences between the differential distribution of cluster ages and the function of the evolutionary fading rate of clusters.

which was noticed in the south-western part of the M31 disk [44]. This might suggest that the second passage of M32 occurred through the present-day south-western part of the disk, and in the area of this study, located on the opposite side of the galaxy, had a minor effect.

The drop of the differential cluster number distribution at ages of ≳400 Myr (Fig. 7) indicates that the characteristic cluster disruption time in the north-eastern part of the M31 disk might be as large as ≳300 Myr, which is in agreement with other studies [9, 44, 54]. However, due to the low number of clusters and the complex interaction between enhanced cluster formation and disruption at these ages, we cannot determine this parameter more accurately.

The deprojected images of massive (>800 $M_{\odot}$) clusters' surface density maps are shown in Fig. 8. To deproject the M31 disk, we applied the position angle of the major axis of 37.7° and the disk inclination of 77.5° [55]. These maps show some circular structures instead of spiral arms. Therefore, let us call them star cluster rings (SCRs). The present-day SCRs are located at the ~6, ~10 and ~15 kpc radial distances from the galaxy's centre; they are estimated from the radial distribution of young (≤100 Myr) and massive (>800 $M_{\odot}$) star clusters (Fig. 9).

The maps of clusters' surface number densities (panels (a) and (c)) and median ages (panels (b) and (d)) in the galaxy disk (Fig. 8) demonstrate a very slow evolution of cluster group structures. The cluster surface number densities kpc^{-2} are colour-coded according to the bar in the middle of the figure; panel (a) shows a younger (≤100 Myr) cluster population, while panel (c) shows an older one ($100 < t \leq 400$ Myr). The median ages (panels (b) and (d)) are colour-coded according to the bars on the right.

The radial profile of cluster surface number density per Myr is shown in Fig. 9. It is calculated for two age ranges within the azimuthal segment of 60° (from −25 to +35° around the major axis). The azimuthal range is limited due to the narrow PHAT survey mapping and our attempt to have a complete coverage of the observed field up to a ~20 kpc distance. The blue line represents younger (≤100 Myr) and the red line shows older ($100 < t \leq 400$ Myr) cluster populations. However, to quantitatively compare the surface number density of younger and older cluster populations, a correction for the fading function should be applied by multiplying the surface number density of the older population by a factor of ~3. This results in about a 2–3 times higher surface number density of older clusters, compared to the present-day population, in the 6 and 10 kpc SCRs. However, the SCR at 15 kpc is visible only as a concentration of younger clusters.

Our results show the younger clusters (≤100 Myr) residing in narrower SCRs compared to the older (>100 Myr) cluster populations. This suggests that clusters form in dense star-forming regions and subsequently disperse into the galaxy. Nonetheless, the fact that this correlation still holds for clusters ~400 Myr old indicates that

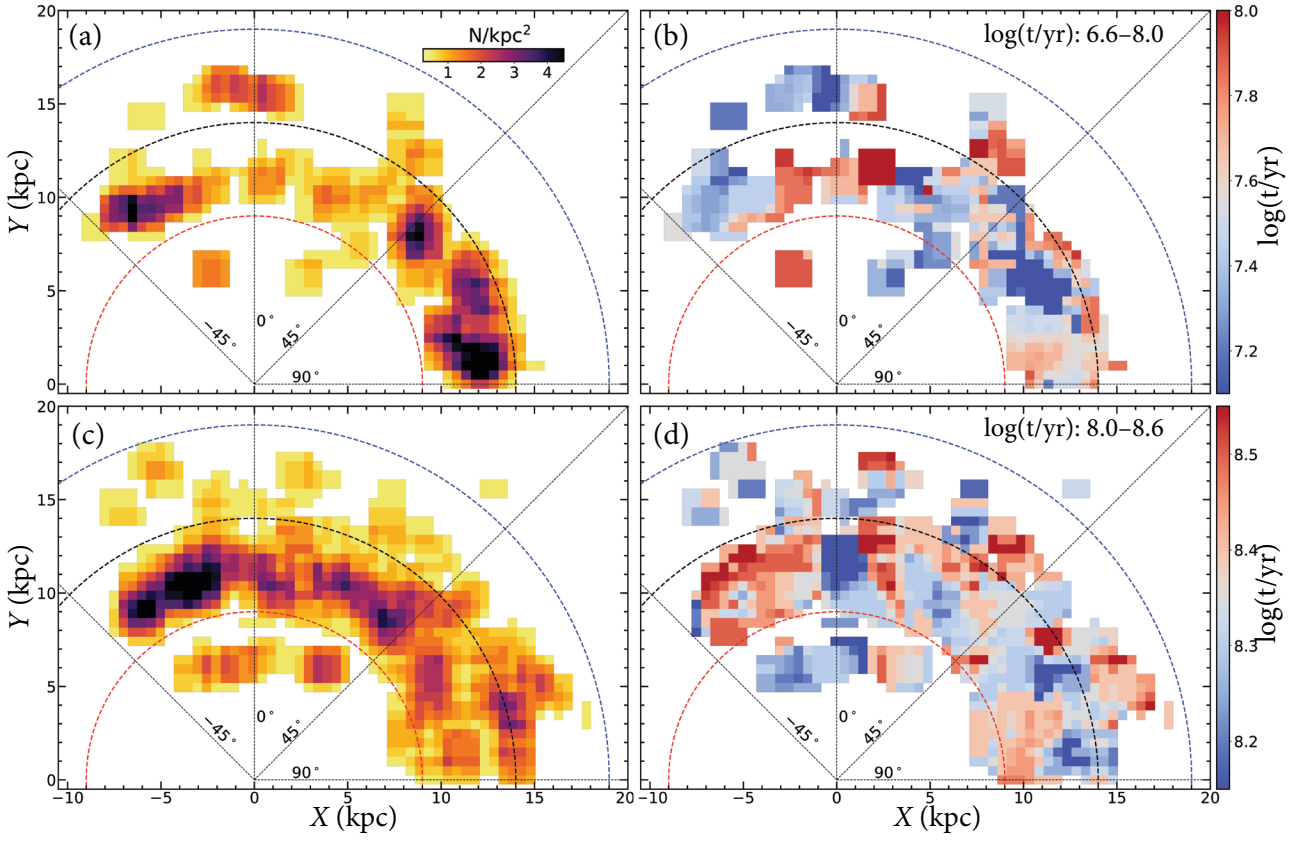

Fig. 8. The maps of massive (>800 $M_\odot$) star clusters' surface number densities (panels (a) and (c)) and median ages (panels (b) and (d)) in the galaxy disk. The cluster number densities kpc^{-2} are colour-coded according to the bar in the middle of the figure; panels (a) and (c) show younger (≤100 Myr) and older (100 < t ≤ 400 Myr) cluster populations, respectively. The median ages (panels (b) and (d)) are colour-coded according to the bars on the right. The vertical coordinate at X = 0.0 corresponds to the major axis of M31. Clusters located in the disk closer to us have negative X coordinates, and the clusters residing on the more distant part of the disk have positive X coordinates. The circles indicate 9, 14 and 19 kpc distances from the galaxy centre.

the dispersion velocity of cluster groups relative to their birthplaces is low. From the differences in concentrations of younger and older cluster populations within the 10 kpc SCR (Figs 8 and 9) we derived an upper limit for the radial spread of cluster groups of ≲0.5 kpc during the ~300 Myr period. This gives a rough estimate of cluster groups' radial velocity dispersion of less than ~2 km/s. Therefore,

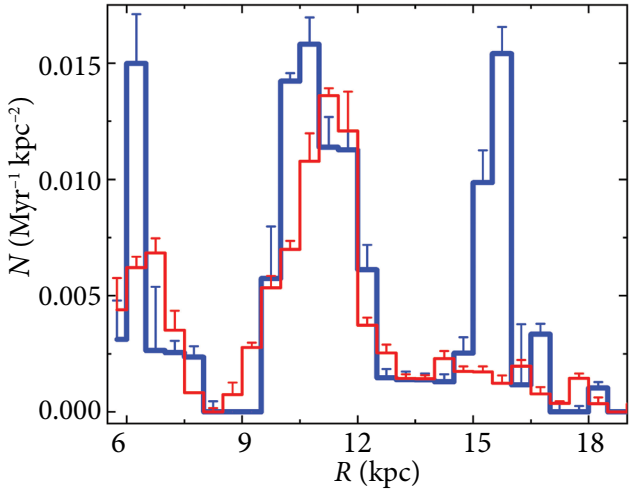

Fig. 9. The radial profiles of massive (>800 $M_\odot$) star clusters' surface number density calculated per Myr in two age ranges within the azimuthal segment of 60° (from −25 to +35°). The blue line represents younger (≤100 Myr) and the red line shows older (100 < t ≤ 400) Myr clusters. The error bars indicate the root-mean-square estimates of data scattering by applying a radial binning procedure.

it suggests star clusters to be very good long-lasting tracers of the star-forming region morphology in disk galaxies.

6. Conclusions

We used the multicolour Panchromatic Hubble Andromeda Treasury (PHAT) survey dataset [11] to derive parameters for a sample of 854 star clusters in the M31 galaxy. For this purpose, we have developed an isochrone fitting procedure for colour-magnitude diagrams of cluster stars. Using the Bayesian method, we derived resolved and semi-resolved star cluster ages and interstellar extinctions.

The determined ages of the clusters indicate that the cluster formation rate in the M31 galaxy was rather constant during the last ~130 Myr. However, at least one active star-forming episode occurred ~220 Myr ago. It might have been induced by the passage of the M32 galaxy through the M31 disk ~210 Myr ago [51].

Derived cluster age distributions in the galaxy show a striking stability of the cluster group locations during the ~300 Myr age interval. Younger and older cluster groups tend to concentrate in the same regions of the galaxy for extended periods of time. This suggests a relatively slow dispersion from their birthplaces. Therefore, clusters are reliable long-lasting tracers not only of the recent star formation history but also of the star-forming region morphology in disk galaxies.

Acknowledgements

We are grateful to the referee for his/her constructive suggestions. This research made use of the following software: TOPCAT (https://www.star.bristol.ac.uk/mbt/topcat); SAOImage DS9 (https://ds9.si.edu); IRAF (https://iraf.net). It is based on observations made with the NASA/ESA Hubble Space Telescope, and obtained from the Hubble Legacy Archive, which is a collaboration between the Space Telescope Science Institute (STScI/NASA), the Space Telescope European Coordinating Facility (STECF/ESA) and the Canadian Astronomy Data Centre (CADC/NRC/CSA). Computations were performed on the supercomputer GALAX of the Center for Physical Sciences and Technology, Lithuania.

References

[1] C.J. Lada and E.A. Lada, Embedded clusters in molecular clouds, Annu. Rev. Astron. Astrophys. **41**, 57 (2003), https://doi.org/10.1146/annurev.astro.41.011802.094844

[2] L.C. Johnson, A.C. Seth, J.J. Dalcanton, L.C. Beerman, M. Fouesneau, A.R. Lewis, D.R. Weisz, B.F. Williams, E.F. Bell, A.E. Dolphin, et al., Panchromatic Hubble Andromeda Treasury. XVI. Star cluster formation efficiency and the clustered fraction of young stars, Astrophys. J. **827**, 33 (2016), https://doi.org/10.3847/0004-637X/827/1/33

[3] T.M. Wainer, L.C. Johnson, A.C. Seth, E.E. TorresVillanueva, J.J. Dalcanton, M.J. Durbin, A. Dolphin, D.R. Weisz, B.F. Williams, and Phatter Collaboration, The Panchromatic Hubble Andromeda Treasury: Triangulum Extended Region (PHATTER). III. The mass function of young stellar clusters in M33, Astrophys. J. **928**, 15 (2022), https://doi.org/10.3847/1538-4357/ac51cf

[4] A.R. Lewis, A.E. Dolphin, J.J. Dalcanton, D.R. Weisz, B.F. Williams, E.F. Bell, A.C. Seth, J.E. Simones, E.D. Skillman, Y. Choi, et al., The Panchromatic Hubble Andromeda Treasury. XI. The spatially resolved recent star formation history of M31, Astrophys. J. **805**, 183 (2015), https://doi.org/10.1088/0004-637X/805/2/183

[5] E.J. Bernard, A.M.N. Ferguson, J.C. Richardson, M.J. Irwin, M.K. Barker, S.L. Hidalgo, A. Aparicio, S.C. Chapman, R.A. Ibata, G.F. Lewis, A.W. McConnachie, and N.R. Tanvir, The nature and origin of substructure in the outskirts of M31 – II. Detailed star formation histories, MNRAS **446**, 2789 (2015), https://doi.org/10.1093/mnras/stu2309

[6] J.J. Dalcanton, B.F. Williams, D. Lang, T.R. Lauer, J.S. Kalirai, A.C. Seth, A. Dolphin, P. Rosenfield, D.R. Weisz, E.F. Bell, et al., The Panchromatic Hubble Andromeda Treasury, Astrophys. J. Suppl. **200**, 18 (2012), https://doi.org/10.1088/0067-0049/200/2/18

[7] L.C. Johnson, A.C. Seth, J.J. Dalcanton, M.L. Wallace, R.J. Simpson, C.J. Lintott, A. Kapadia,

E.D. Skillman, N. Caldwell, M. Fouesneau, et al., PHAT Stellar Cluster Survey. II. Andromeda Project Cluster Catalog, Astrophys. J. **802**, 127 (2015), https://doi.org/10.1088/0004-637X/802/2/127

[8] P. de Meulenaer, D. Narbutis, T. Mineikis, and V. Vansevičius, Deriving physical parameters of unresolved star clusters. III. Application to M31 PHAT clusters, Astron. Astrophys. **574**, A66 (2015), https://doi.org/10.1051/0004-6361/201425121

[9] P. de Meulenaer, R. Stonkutė, and V. Vansevičius, Deriving physical parameters of unresolved star clusters. V. M31 PHAT star clusters, Astron. Astrophys. **602**, A112 (2017), https://doi.org/10.1051/0004-6361/201730751

[10] A. Bridžius, D. Narbutis, R. Stonkutė, V. Deveikis, and V. Vansevičius, Accuracy of star cluster parameters from integrated UBVRIJHK photometry, Balt. Astron. **17**, 337 (2008), https://doi.org/10.48550/arXiv.0902.3167

[11] B.F. Williams, M. Durbin, D. Lang, J.J. Dalcanton, A.E. Dolphin, A. Smercina, P. Yanchulova Merica-Jones, D.R. Weisz, E.F. Bell, K.M. Gilbert, et al., The Panchromatic Hubble Andromeda Treasury. XXI. The Legacy Resolved Stellar Photometry Catalog, Astrophys. J. Suppl. **268**, 48 (2023), https://doi.org/10.3847/1538-4365/acea61

[12] R. Naujalis, R. Stonkutė, and V. Vansevičius, Deriving physical parameters of unresolved star clusters. VI. Adaptive aperture photometry of the M31 PHAT star clusters, Astron. Astrophys. **654**, A6 (2021), https://doi.org/10.1051/0004-6361/202039306

[13] E. Kriščiūnas, K. Daugevičius, R. Stonkutė, and V. Vansevičius, Deriving physical parameters of unresolved star clusters. VII. Adaptive aperture photometry of the M31 PHAT star clusters, Astron. Astrophys. **677**, A100 (2023), https://doi.org/10.1051/0004-6361/202347140

[14] C. Bonatto and E. Bica, Investigating the age and structure of the infrared old open clusters LK1, LK10, FSR1521 and FSR1555, MNRAS **392**, 483 (2009), https://doi.org/10.1111/j.1365-2966.2008.14093.x

[15] E.R. Garro, D. Minniti, M. Gómez, J.G. Fernández-Trincado, J. Alonso-García, M. Hempel, and R. Zelada Bacigalupo, A new low-luminosity globular cluster discovered in the Milky Way with the VVVX survey, Astron. Astrophys. **662**, A95 (2022), https://doi.org/10.1051/0004-6361/202243342

[16] A.B. Pace, S.E. Koposov, M.G. Walker, N. Caldwell, M. Mateo, E.W. Olszewski, I.U. Roederer, J.I. Bailey, V. Belokurov, K. Kuehn, T.S. Li, and D.B. Zucker, The kinematics, metallicities, and orbits of six recently discovered Galactic star clusters with Magellan/M2FS spectroscopy, MNRAS **526**, 1075 (2023), https://doi.org/10.1093/mnras/stad2760

[17] S. Sandrelli, A. Bragaglia, M. Tosi, and G. Marconi, The intermediate age open cluster NGC 2660, MNRAS **309**, 739 (1999), https://doi.org/10.1046/j.1365-8711.1999.02906.x

[18] M. Cignoni, G. Beccari, A. Bragaglia, and M. Tosi, Three new bricks in the wall: Berkeley 23, Berkeley 31 and King 8, MNRAS **416**, 1077 (2011), https://doi.org/10.1111/j.1365-2966.2011.19104.x

[19] C. Bonatto, E. Bica, and E.F. Lima, Deriving reliable fundamental parameters of pre-main-sequence-rich star clusters affected by differential reddening, MNRAS **420**, 352 (2012), https://doi.org/10.1111/j.1365-2966.2011.20039.x

[20] W.L. Sanders, An improved method for computing membership probabilities in open clusters, Astron. Astrophys. **14**, 226 (1971).

[21] L.M. Sarro, H. Bouy, A. Berihuete, E. Bertin, E. Moraux, J. Bouvier, J.C. Cuillandre, D. Barrado, and E. Solano, Cluster membership probabilities from proper motions and multi-wavelength photometric catalogues. I. Method and application to the Pleiades cluster, Astron. Astrophys. **563**, A45 (2014), https://doi.org/10.1051/0004-6361/201322413

[22] J.J. Claria and E. Lapasset, Fundamental parameters of the open cluster NGC 2567, Astron. J. **91**, 326 (1986), https://doi.org/10.1086/114013

[23] J. Roberts, C. Lewis, D.R. Gies, J.R. Parks, E.D. Grundstrom, M.V. McSwain, D.H. Berger, B.D. Mason, T.A. ten Brummelaar, and N.H. Turner, The membership and distance of the open Cluster Collinder 419, Astron. J. **140**, 744 (2010), https://doi.org/10.1088/0004-6256/140/3/744

[24] M. Mateo and P. Hodge, CCD photometry of Large Magellanic Cloud clusters. II. The Intermediate-Age Cluster H4, Astrophys. J. Suppl. **60**, 893 (1986), https://doi.org/10.1086/191104

[25] C. Bonatto and E. Bica, Open clusters in dense fields: the importance of field-star decontamination for NGC 5715, Lyngå 4, Lyngå 9, Trumpler 23, Trumpler 26 and Czernik 37, MNRAS **377**, 1301 (2007), https://doi.org/10.1111/j.1365-2966.2007.11691.x

[26] A.E. Piatti and E. Bica, Washington photometry of candidate star clusters in the Small Magellanic Cloud, MNRAS **425**, 3085 (2012), https://doi.org/10.1111/j.1365-2966.2012.21694.x

[27] A. Krone-Martins and A. Moitinho, UPMASK: unsupervised photometric membership assignment in stellar clusters, Astron. Astrophys. **561**, A57 (2014), https://doi.org/10.1051/0004-6361/201321143

[28] M.S. Pera, G.I. Perren, A. Moitinho, H.D. Navone, and R.A. Vazquez, pyUPMASK: an improved unsupervised clustering algorithm, Astron. Astrophys. **650**, A109 (2021), https://doi.org/10.1051/0004-6361/202040252

[29] H. Monteiro, W.S. Dias, and T.C. Caetano, Fitting isochrones to open cluster photometric data. A new global optimization tool, Astron. Astrophys. **516**, A2 (2010), https://doi.org/10.1051/0004-6361/200913677

[30] D.B. Pavani, L.O. Kerber, E. Bica, and W.J. Maciel, Diagnostic tool to analyse colour-magnitude diagrams of poorly populated stellar concentrations, MNRAS **412**, 1611 (2011), https://doi.org/10.1111/j.1365-2966.2010.17999.x

[31] T. Cantat-Gaudin, A. Vallenari, R. Sordo, F. Pensabene, A. Krone-Martins, A. Moitinho, C. Jordi, L. Casamiquela, L. Balaguer-Núnez, C. Soubiran, and N. Brouillet, Characterising open clusters in the solar neighbourhood with the Tycho-Gaia Astrometric Solution, Astron. Astrophys. **615**, A49 (2018), https://doi.org/10.1051/0004-6361/201731251

[32] L.O. Kerber, B.X. Santiago, R. Castro, and D. Valls-Gabaud, Analysis of colour-magnitude diagrams of rich LMC clusters: NGC 1831, Astron. Astrophys. **390**, 121 (2002), https://doi.org/10.1051/0004-6361:20020692

[33] G.I. Perren, R.A. Vázquez, and A.E. Piatti, ASteCA: Automated Stellar Cluster Analysis, Astron. Astrophys. **576**, A6 (2015), https://doi.org/10.1051/0004-6361/201424946

[34] J. Bialopetravičius, D. Narbutis, and V. Vansevičius, Deriving star cluster parameters with convolutional neural networks. I. Age, mass, and size, Astron. Astrophys. **621**, A103 (2019), https://doi.org/10.1051/0004-6361/201833833

[35] A.W. McConnachie, M.J. Irwin, A.M.N. Ferguson, R.A. Ibata, G.F. Lewis, and N. Tanvir, Distances and metallicities for 17 Local Group galaxies, MNRAS **356**, 979 (2005), https://doi.org/10.1111/j.1365-2966.2004.08514.x

[36] P. Kroupa, On the variation of the initial mass function, MNRAS **322**, 231 (2001), https://doi.org/10.1046/j.1365-8711.2001.04022.x

[37] A. Bressan, P. Marigo, L. Girardi, B. Salasnich, C. Dal Cero, S. Rubele, and A. Nanni, PARSEC: stellar tracks and isochrones with the PAdova and TRieste Stellar Evolution Code, MNRAS **427**, 127 (2012), https://doi.org/10.1111/j.1365-2966.2012.21948.x

[38] P. Marigo, L. Girardi, A. Bressan, P. Rosenfield, B. Aringer, Y. Chen, M. Dussin, A. Nanni, G. Pastorelli, T.S. Rodrigues, et al., A new generation of PARSEC-COLIBRI stellar isochrones including the TP-AGB phase, Astrophys. J. **835**, 77 (2017), https://doi.org/10.3847/1538-4357/835/1/77

[39] N.E. Sanders, N. Caldwell, J. McDowell, and P. Harding, The metallicity profile of M31 from spectroscopy of hundreds of H II regions and PNe, Astrophys. J. **758**, 133 (2012), https://doi.org/10.1088/0004-637X/758/2/133

[40] A. Zurita and F. Bresolin, The chemical abundance in M31 from H II regions, MNRAS **427**, 1463 (2012), https://doi.org/10.1111/j.1365-2966.2012.22075.x

[41] E.F. Schlafly and D.P. Finkbeiner, Measuring reddening with sloan digital sky survey stellar spectra and recalibrating SFD, Astrophys. J. **737**, 103 (2011), https://doi.org/10.1088/0004-637X/737/2/103

[42] P.J. Brown and T. Walker, Galaxian contamination in galactic reddening maps, Astron. J. **163**, 14 (2022), https://doi.org/10.3847/1538-3881/ac32cb

[43] L.C. Johnson, T.M. Wainer, E.E. Torresvillanueva, A.C. Seth, B.F. Williams, M.J. Durbin, J.J. Dalcanton, D.R. Weisz, E.F. Bell, P. Guhathakurta, E. Skillman, A. Smercina, and Phatter Collaboration, The Panchromatic Hubble Andromeda Treasury: Triangulum Extended Region (PHATTER). IV. Star Cluster Catalog, Astrophys. J. **938**, 81 (2022), https://doi.org/10.3847/1538-4357/ac8def

[44] V. Vansevičius, K. Kodaira, D. Narbutis, R. Stonkutė, A. Bridžius, V. Deveikis, and D. Semionov, Compact star clusters in the M31 Disk, Astrophys. J. **703**, 1872 (2009), https://doi.org/10.1088/0004-637X/703/2/1872

[45] P. de Meulenaer, D. Narbutis, T. Mineikis, and V. Vansevičius, Deriving physical parameters of unresolved star clusters. I. Age, mass, and extinction degeneracies, Astron. Astrophys. **550**, A20 (2013), https://doi.org/10.1051/0004-6361/201220674

[46] P. de Meulenaer, D. Narbutis, T. Mineikis, and V. Vansevičius, Deriving physical parameters of unresolved star clusters. II. The degeneracies of age, mass, extinction, and metallicity, Astron. Astrophys. **569**, A4 (2014), https://doi.org/10.1051/0004-6361/201423988

[47] S.G. Boutloukos and H.J.G.L.M. Lamers, Star cluster formation and disruption time-scales – I. An empirical determination of the disruption time of star clusters in four galaxies, MNRAS **338**, 717 (2003), https://doi.org/10.1046/j.1365-8711.2003.06083.x

[48] H.J.G.L.M. Lamers, M. Gieles, and S.F. Portegies Zwart, Disruption time scales of star clusters in different galaxies, Astron. Astrophys. **429**, 173 (2005), https://doi.org/10.1051/0004-6361:20041476

[49] K. Kodaira, V. Vansevičius, A. Bridžius, Y. Komiyama, S. Miyazaki, R. Stonkutė, I. Šablevičiūtė, and D. Narbutis, A survey of compact star clusters in the south-west field of the M31 disk, Publ. Astron. Soc. Jpn. **56**, 1025 (2004), https://doi.org/10.1093/pasj/56.6.1025

[50] D. Narbutis, V. Vansevičius, K. Kodaira, A. Bridžius, and R. Stonkutė, A survey of star clusters in the M31 southwest field: UBVRI photometry and multiband maps, Astrophys. J. Suppl. **177**, 174 (2008), https://doi.org/10.1086/586736

[51] D.L. Block, F. Bournaud, F. Combes, R. Groess, P. Barmby, M.L.N. Ashby, G.G.Fazio, M.A. Pahre, and S.P. Willner, An almost head-on collision as the origin of two off-centre rings in the Andromeda galaxy, Nature **443**, 832 (2006), https://doi.org/10.1038/nature05184

[52] S. Wang, J. Ma, Z. Fan, Z. Wu, T. Zhang, H. Zou, and X. Zhou, Age and mass studies for young star clusters in M31 from SEDS-FIT, Astron. J. **144**, 191 (2012), https://doi.org/10.1088/0004-6256/144/6/191

[53] M. Dierickx, L. Blecha, and A. Loeb, Signatures of the M31–M32 galactic collision, Astrophys. J. Lett. **788**, L38 (2014), https://doi.org/10.1088/2041-8205/788/2/L38

[54] L.C. Johnson, A.C. Seth, J.J. Dalcanton, L.C. Beerman, M. Fouesneau, D.R. Weisz, T.A. Bell, A.E. Dolphin, K. Sandstrom, and B.F. Williams, Panchromatic Hubble Andromeda Treasury. XVIII. The high-mass truncation of the star cluster mass function, Astrophys. J. **839**, 78 (2017), https://doi.org/10.3847/1538-4357/aa6a1f

[55] P.W. Hodge, *The Andromeda Galaxy*, Astrophysics and Space Science Library, Vol. 176 (Springer, Netherlands, 1992) p. viii.

ANDROMEDOS GALAKTIKOS DISKO ŽVAIGŽDŽIŲ SPIEČIŲ POPULIACIJOS EVOLIUCIJA

M. Čeponis [a], R. Stonkutė [a, b], V. Vansevičius [a]

[a] *Fizinių ir technologijos mokslų centras, Vilnius, Lietuva*

[b] *Vilniaus universiteto astronomijos observatorija, Vilnius, Lietuva*

Santrauka

Tiksliausiai žvaigždžių spiečių parametrai nustatomi analizuojant jų žvaigždžių spalvos ir ryškio diagramas (angl. *colour-magnitude diagram*s, CMD). Neseniai šis būdas buvo panaudotas „Panchromatic Hubble Andromeda Treasury“ (PHAT) apžvalgos žvaigždžių spiečių iki 300 mln. m. amžiaus tyrimui. Šiame darbe, naudodami savo sukurtą žvaigždžių spiečių amžiaus ir tarpžvaigždinės ekstinkcijos nustatymo metodą, išplėtėme tiriamų žvaigždžių spiečių amžiaus ribą iki 700 mln. m. Atlikome 854 žvaigždžių spiečių imties iš PHAT apžvalgos analizę. Parodėme, kad žvaigždžių spiečių formavimosi greitis Andromedos galaktikoje (M31) buvo pastovus pastaruosius 130 mln. m. Tačiau nustatėme reikšmingą žvaigždėdaros suaktyvėjimą, įvykusį prieš ~220 mln. m., kuris gali būti siejamas su M32 galaktikos perėjimu per M31 diską.